Calle, Miguel A. G.; Salmi, Mika; Mazzariol, Leonardo M.; Kujala, Pentti

Miniature reproduction of raking tests on marine structure: Similarity technique and experiment

Published in:
Engineering Structures

DOI:
10.1016/j.engstruct.2020.110527

Published: 01/06/2020

Document Version
Early version, also known as pre-print

Please cite the original version:
Calle, M. A. G., Salmi, M., Mazzariol, L. M., & Kujala, P. (2020). Miniature reproduction of raking tests on marine structure: Similarity technique and experiment. *Engineering Structures*, *212*, Article 110527. https://doi.org/10.1016/j.engstruct.2020.110527

Miniature reproduction of raking test of marine structure: Similarity technique and experiment

Miguel A. G. Calle*,, Mika Salmi***, Leonardo M. Mazzariol**, Pentti Kujala***

*Marine Technology Research Group, Department of Mechanical Engineering, Aalto University, Tietotie 1C, 02150, Espoo, Finland

**Engineering Modeling and Applied Social Sciences (CECS), Federal University of ABC, Av. Dos Estados, 5001, Santo André - SP, 09210-580, Brazil

***Advanced Manufacturing and Materials Research Group, Department of Mechanical Engineering, Aalto University, Otakaari 4, 02150, Espoo, Finland

Abstract

Substantial progress has been made in the last decades to computationally model the structural response of marine structures subjected to collision and grounding accidents. The finite element method stands out as the most reliable and robust technique within other tools for this purpose. However, there are still some complex physical aspects arduous to be modeled numerically. This work presents an experimental technique to reproduce the mechanical response and collapse mode of marine structures subjected to collision and grounding events by using miniature models built by additive manufacturing. This experimental technique relies on structural scaling and thickness distortion formulations. A raking test of a large-scale ship bottom was replicated in 1:30 reduced scale to validate this technique. The miniature ship bottom structure was additively manufactured from stainless steel 316L considering all structural details. Flat dog-bone samples with different thicknesses were also built in the same way for mechanical characterization of the material via tensile tests and microscopy analysis of material fractures. Tensile tests showed a good consistency in stress-strain curves with a small, but noteworthy, influence of plate thickness and a large dispersion in rupture elongations. The fractured sections revealed various void formations around non-sintered metal powder. In spite of that, the structural response obtained from miniature test showed a good correspondence with the large-scale reference test when both are brought to the same dimensional scale.

Keywords: Additive Manufacturing; Raking Test; Similarity; Powder Bed Fusion; Steel 316L

1. Background

Naval accidents involving collision and grounding of oil tanker ships are responsible for a high percentage of marine oil spill disasters. In the past, different lines of action were developed to predict the structural consequences of such kind of events mainly based on empirical methods, simplified analytical formulations and reduced-scale experiments. Since the 1990s, the recent progress in computational power made viable the non-linear finite element (FE) modeling of partial or entire marine structures subjected to collision or grounding events. However, so far, the FE modeling of some aspects are still very arduous to manage and include such as the ship cargo, hydrodynamic effect of the surrounding water and oil spill occurrence among others.

Few experimental researches were able to model a ship collision and ship grounding scenarios with surrounding water. Tabri et al. (2008, 2009) reproduced ship collision events by using miniature wooden ships with deformable foam laterals in the contact interface in order to replicate the structural crushing response. Recently, Zhu et al. (2018) reproduced ship grounding events using a miniature simplified ship model with a flat bottom plate. In both cases, these studies were able to mimic the rigid body dynamics of the ship(s), but lacking in reproducing the real structural collapse of the represented structures.

In this sense, Calle et al. (2017) and Oshiro et al. (2017) were able to build complex miniature marine structures in 1:100 scale using thin mild steel plates cut and welded by laser, but at cost of some geometry simplifications and exclusion of structural details such as stiffeners, connections and cutouts. In spite of these limitations, the tests with these models allowed to reproduce coarsely the collapse mode of oil tanker structures subjected to collision and grounding events in dry conditions, as well as to evaluate the efficacy of failure criteria purposely developed for ship collision events (Calle et al., 2019a).

With the aim of building miniature marine structures with geometries as faithful as possible to complex real-scale structures, additive manufacturing (AM) techniques within Powder Bed Fusion (PBF) processes are here utilized (ISO/ASTM 52900, 2015). In PBF process of metals, the part is built up by melting metal powder layer after layer according to a three-dimensional CAD model. The main advantage of AM techniques is the capability to create complex geometries involving barely one manufacturing stage. Although, to generate functional parts for structural purposes, post-processing such as surface finishing, heat treatments, material densification among others are necessary (Calle et al., 2019). In industry, the resulting poor surface quality is been seen as one of the biggest technical barrier for utilizing the AM technologies (Kretzschmar et al., 2018).

The objective of this work is to present an experimental technique to reproduce the structural response and collapse mode of the raking test of a real ship tanker structure, but in miniature scale. Similarity laws with geometry distortion establish the correspondence between the real scale test (prototype) variables and those of the miniature test (model) as presented in Section 2. The raking test of the large-scale marine structure used as reference in this work (Kuroiwa et al., 1992) is fully described in Section 3. The manufacture of the miniature marine structure by AM and the mechanical characterization of its material is presented in Section 4. Finally, the comparison between the structural responses of the miniature and large-scale raking tests as well as the conclusions of this research are presented in Sections 5 and 6, respectively.

2. Scaling and thickness distortion

The similarity is the technique employed to reproduce certain mechanical/structural event, here called as prototype, in a different dimensional scale by a model. The correspondence between the physical variables of the prototype and model is given by the scaling factors and they, in turn, are obtained from dimensional analysis and Buckingham π-theorem assuming that both, prototype and model, have the same relevant quantities (same mechanical properties). This set of scaling factors are also called as the Cauchy similarity law or Mass-Length-Time basis similarity law (MLT).

However, these scaling factors are not fully effective when modeling structural collision events due to the distortion induced by some mechanical properties of the material such as viscoplasticity, failure and density. These errors on similarity increase when the mechanical properties of the model differ, to some extent, from that of the prototype. To amend them, the Velocity-yield Stress-Mass-Density basis similarity law (VSG-D), purposely developed for similarity in structural impact events by Mazzariol et al. (2016), is here employed.

Here is also presented a thickness distortion technique to increase (distort) the plate thickness of the miniature structure model to dimensions suitable for AM without altering the structural collapse mode when compared against the reference non-distorted structure.

A uniform increase in the thicknesses of all structural members would not generate a proportional increase in the reaction force of each one of the structural members so altering, even drastically, the overall collapse mode.

To deal with it, the thickness of each structural member is distorted in a different manner in line with its expected dominant structural collapse. According to studies on collision of marine structures

(Liu et al., 2018), most of the collapse modes observed in structural members can be grouped into three categories (or a combination of them): membrane tension, folding and tearing.

In this technique, the collapse modes of each structural member need to be assumed beforehand. According to analytical models on structural collapse, the reaction force of a thin-walled structural member when subjected to pure membrane tension is directly proportional to its thickness, when subjected to folding, to its thickness raised to 5/3, and, when subjected to tearing, to its thickness raised to 3/2 (See Appendix A). Besides, these reaction forces are also directly proportional to the material yield stress in any case, Table 1.

The reaction force of each one of the original structural members is presented in terms of the yield stress and plate thickness. Then, the reaction forces of each structural member with distorted thickness and different flow stress can be easily expressed by including additional terms in the original expressions as shown in Table 1. These additional terms can be extracted from the sum so isolating them from the original form. To induce proportional increase in the reaction force of each structural members (and, consequently, in the total force) these additional terms are equated (as shown in the “Equation distortion term” column in Table 1). Finally, the thickness distortion factors are presented as a function of η and their flow stress ratios as summarized in Table 1.

Both scaling and thickness distortion techniques are coupled to be applied together in sequence (regardless of the order). In order to validate this method, a miniature model is designed and manufactured based on a real scale test (prototype) using this coupled technique. After subjecting the model to mechanical testing, its structural response is verified by bringing it to its real scale equivalent (also via coupled technique) and comparing against the prototype’s structural response as schematized in Fig. 1. Table 2 summarizes the scaling factors for physical variables that are relevant for quasi-static modeling according to the coupled technique.

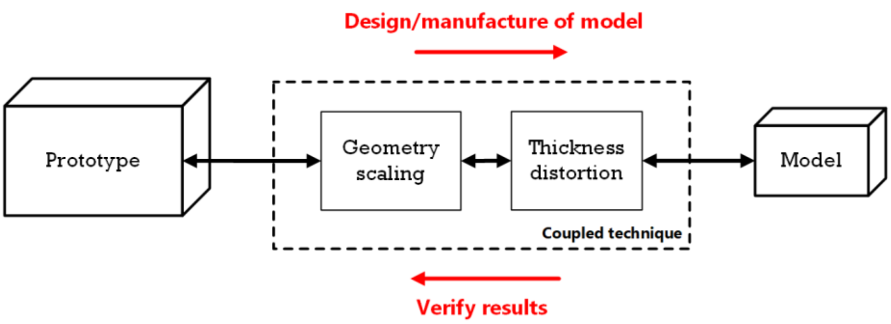

Fig. 1. Scaling and thickness distortion techniques.

Table 1. Formulations for thickness distortion technique

Structural members by collapse mode	Proportionality of force	$\sum F$ in original structural members	$\sum F$ in structural members with distorted thickness		Equating distortion term	Thickness distortion of each structural member
			General form	Balanced first term		
Membrane tension	$\bar{F}_m \propto \sigma_0\, t$	$\sum_{i=1}^{I} k_{m,i}\, \sigma_{0,i}\, t_i$	$\sum_{i=1}^{I} k_{m,i}\, \sigma_0 \left(\frac{\sigma_{0,i}}{\sigma_0}\right)(\eta_{t,m}\, t_i)$	$\left(\frac{\sigma_{0,i}}{\sigma_0}\right)\eta_{t,m} \sum_{i=1}^{I} k_{m,i}\, \sigma_0\, t_i$	$\left(\frac{\sigma_{0,i}}{\sigma_0}\right)\eta_{t,m}$	$\eta_{t,m} = \left(\frac{\sigma_{0,i}}{\sigma_0}\right)^{-1} \eta^{5/3}$
Folding	$\bar{F}_f \propto \sigma_0\, t^{5/3}$	$\sum_{j=1}^{J} k_{f,j}\, \sigma_{0,j}\, t_j^{5/3}$	$\sum_{j=1}^{J} k_{f,j}\, \sigma_0 \left(\frac{\sigma_{0,j}}{\sigma_0}\right)(\eta_{t,f}\, t_j)^{5/3}$	$\left(\frac{\sigma_{0,j}}{\sigma_0}\right)\eta_{t,f}{}^{5/3} \sum_{j=1}^{J} k_{f,j}\, \sigma_0\, t_j{}^{5/3}$	$\left(\frac{\sigma_{0,j}}{\sigma_0}\right)(\eta_{t,f})^{5/3}$	$\eta_{t,f} = \left(\frac{\sigma_{0,j}}{\sigma_0}\right)^{-3/5} \eta$
Tearing	$\bar{F}_t \propto \sigma_0\, t^{3/2}$	$\sum_{k=1}^{K} k_{t,k}\, \sigma_{0,k}\, t_k^{3/2}$	$\sum_{k=1}^{K} k_{t,k}\, \sigma_0 \left(\frac{\sigma_{0,k}}{\sigma_0}\right)(\eta_{t,t}\, t_k)^{3/2}$	$\left(\frac{\sigma_{0,k}}{\sigma_0}\right)\eta_{t,t}{}^{3/2} \sum_{k=1}^{K} k_{t,k}\, \sigma_0\, t_k{}^{3/2}$	$\left(\frac{\sigma_{0,k}}{\sigma_0}\right)\eta_{t,t}{}^{3/2}$	$\eta_{t,t} = \left(\frac{\sigma_{0,k}}{\sigma_0}\right)^{-2/3} \eta^{10/9}$
All	-	$\sum F$	$\sum F_{distort} = \sum \eta_F\, F$	$\sum F_{distort} = \eta_F \sum F$	η_F	$\eta_F = \eta^{5/3}$

Table 2. Coupled factors for dimensional scaling and thickness distortion.

Variable	Symbol	Factors
Length	β	β
Thickness	η_t	$\left(\frac{\sigma_{0,i}}{\sigma_0}\right)^{-1} \eta^{5/3}$ (membrane tension) $\left(\frac{\sigma_{0,j}}{\sigma_0}\right)^{-3/5} \eta$ (folding) $\left(\frac{\sigma_{0,k}}{\sigma_0}\right)^{-2/3} \eta^{10/9}$ (tearing)
displacement	β_δ	β
Force	β_F	$\eta^{5/3}\, \beta_{\sigma_0}\, \beta_{\sigma_{visco}}\, \beta^2$
Energy	β_E	$\eta^{5/3}\, \beta_{\sigma_0}\, \beta_{\sigma_{visco}}\, \beta^3$

β is the scale factor defined by $\beta = (L)_m/(L)_p$.

η is a factor to distort thickness and the resulting distortion is dependent on the collapse mode.

i, j and k are numbers used to identify each structural member.

$\beta_{\sigma_{visco}}$ is a non-dimensional factor that amend the distortion induced by the material viscoplasticity and depends on the chosen viscoplasticity model. In the case of quasi-static tests, this parameter can be assumed as 1.0.

β_{σ_0} is a non-dimensional factor that relates the flow stresses of the model and prototype materials in the form $\beta_{\sigma_0} = (\sigma_0)_m/(\sigma_0)_p$. The value of this factor is strongly dependent on how flow stress is defined. Previous analysis (Calle et al., 2019) corroborated a good similarity correspondence when considering β_{σ_0} not as a single factor, but as a range (Eq. 1), in which the flow stress is evaluated as the yield stress (lower bound) and as the average of yield stress and ultimate tensile strength (upper bound):

$$\frac{[\sigma_{\mathrm{y}}]_m}{[\sigma_{\mathrm{y}}]_p} \leq \beta_{\sigma_0} \leq \frac{[0.5\,(\sigma_{\mathrm{y}}+\sigma_{\mathrm{UTS}})]_m}{[0.5\,(\sigma_{\mathrm{y}}+\sigma_{\mathrm{UTS}})]_p} \qquad (1)$$

3. Reference large-scale test

In 1993, the Association for Structural Improvement of Shipbuilding Industry (ASIS) of Japan carried out two static raking tests in a scaled ship bottom structure as parts of the research project

"Protection of oil spills from crude oil tankers" (Ohtsubo, 1994) with the aim to study numerically the failure mechanism of marine structures. The structure aimed to reproduce a section of a single-plate bottom structure of a VLCC oil tanker (Very Large Crude Carrier) in 1:3 scale from the limitation of the test apparatus capacity (Kuroiwa et al., 1992).

A wedge-shaped rigid rock model indents laterally a ship bottom structure and penetrates along the direction of the ship length as means to represent a ship grounding occurrence. Fig. 2 shows a schematic view of the experiment. The ship bottom structure consists in a longitudinally stiffened bottom plate together with a stiffened transversal ring. Kuroiwa et al. (1992) and Törnqvist (2003) portrayed most of the structural dimensions for the ship bottom structure as well as thicknesses and mechanical properties of each structural member as listed in Table 3.

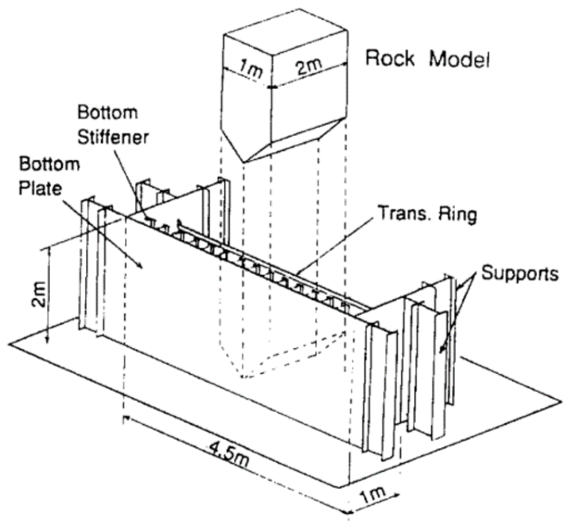

Fig. 2. Scheme of reference large-scale experiment (Kuroiwa et al., 1992).

The structure has general dimensions of 4.5 m width × 2.0 m height × 1.0 m depth. Weld beads were also scaled by 1/3 so implementing a global leg length of 3.0 mm for all welded joints (Kuroiwa et al., 1992). The tip angle of the wedge was 90 degrees. The indentation velocity of the rock model was 0.76 mm/s. Despite the original experimental data included the strains histories in several key points of the structure, only the raking force versus rock displacement data for one test was found available (Kuroiwa et al., 1992).

In the experiment, most of the structural damage occurs under the wedge leaving the rest of the structure practically undamaged. At about 400 mm penetration, the wedge hits the transversal ring and the reaction force increases quickly up to a maximum peak when a penetration of 520 mm is achieved. The dominating collapse mode observed in most of the structural members (that contributes with the reaction force) is tearing. Besides, some failure of the fillet welding between bottom shell and stiffeners and between transversal ring web/face and stiffeners were observed as stated by Kuroiwa et al. (1992).

Table 3. Material parameters for each structural member of the reference large-scale structure.

Structural member	Plate thickness (mm)	Yield stress (MPa)	K (MPa)	n (-)	UTS (MPa)
Bottom shell	7.0	295	720	0.24	402.1
Longitudinal stiffener web	6.0	315	720	0.23	408
Longitudinal stiffener flange	9.0	295	780	0.24	435.6
Transversal ring web	5.0	315	720	0.23	408
Transversal ring stiffener	4.5	315	720	0.23	408
Transversal ring face	9.0	295	780	0.24	435.6

K and n are material parameters according to the power law constitutive model ($\sigma = K\varepsilon^n$)

UTS (Ultimate tensile strength) is evaluated by $\sigma_{UTS} = K(n/\mathrm{e})^n$ where e = 2.7183

4. Miniature model

4.1. Concept

A reduction scale of 1:30 was adopted to reproduce the raking test of the single-plate ship bottom structure previously presented. This scale actually corresponds to a reduction of 1:90 from a real VLCC tanker's bottom structure because a 1:3 scale was already used in the large-scale reference test. However, a geometrical reduction of 30 times of the reference experiment would result in a structure with plate thicknesses between 0.15 and 0.3 mm as better detailed in Table 8.

The thickness distortion technique is used to increase the thicknesses of the structural members of the miniature model to possible made by AM and functional values that range from 0.3 to 0.4 mm. To be coherent with the large-scale ship bottom collapse reported by Kuroiwa et al. (1992), it is assumed that the structural members oriented transversally and that come into direct contact with the wedge angle will undergoes predominately tearing. Complementarily, the structural members oriented longitudinally are assumed to collapse by folding. Then, the wall thickness of each structural member is distorted according to the technique presented previously. The η factor is assumed as 2.2 (and σ_0 as 315 MPa) so to get printable structural members with minimum thickness of 0.33 mm. The resulting thicknesses' distortion are shown in Table 8. The weld beads were also enlarged to be consistent with the plate thickening, but not according to a specific collapse mode or flow stress ratio as shown in Table 8.

Table 4. Thicknesses evaluation for each structural member of the miniature structure.

#	Structural member	Dominant collapse mode	Prototype thickness (mm)	1:30 scaled thickness (mm)	Flow stress ratio	Thickness distortion η_t	Model thickness (mm)
1	Bottom shell	Tearing	7.0	0.233	0.964	2.460	0.57
2	Longitudinal stiffener web	Folding	6.0	0.2	1.0	2.2	0.44
3	Longitudinal stiffener flange	Folding	9.0	0.3	1.011	2.186	0.66
4	Transversal ring web	Tearing	5.0	0.166	1.0	2.401	0.4
5	Transversal ring stiffener	Folding	4.5	0.15	1.0	2.2	0.33
6	Transversal ring face	Tearing	9.0	0.3	1.011	2.385	0.72
7	Weld bead	-	3.0	0.1	-	2.4	0.24

Constructive details such as welded joints and cutouts in the intersections of the structural members are reproduced according technical drawing published by Kuroiwa et al. (1992), Fig. 3. Cutouts and structural details are also reproduced following specifications of marine structure standards (Jordan and Krumpen, 1985). No assembly misalignment or pre-folded collapse pattern are included in the miniature model geometry.

An extended plate border is included in the lateral and bottom edges of the miniature structure to clamp it to the rigid support during the raking test, Fig. 4. This extension counts on draw beads to avoid structural slipping during the raking test. At the same time, the structure has a 1 mm thick frame to give stability to the miniature structure during its manufacture, Fig. 4.

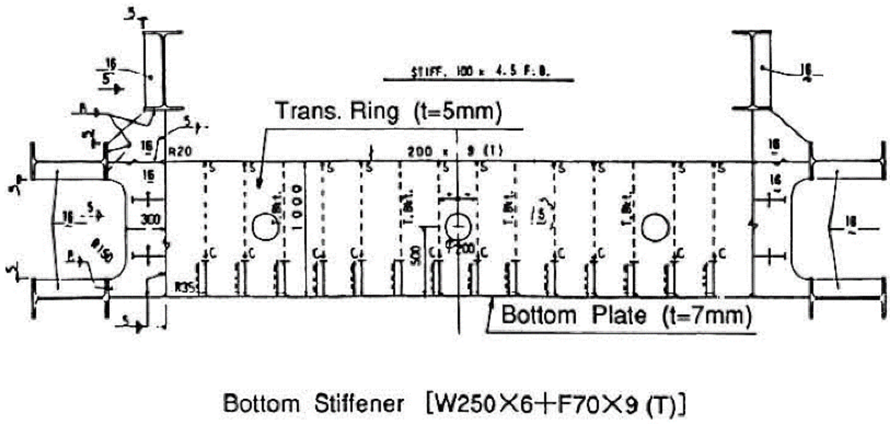

Fig. 3. Top view of single-plate ship bottom structure (Kuroiwa et al., 1992).

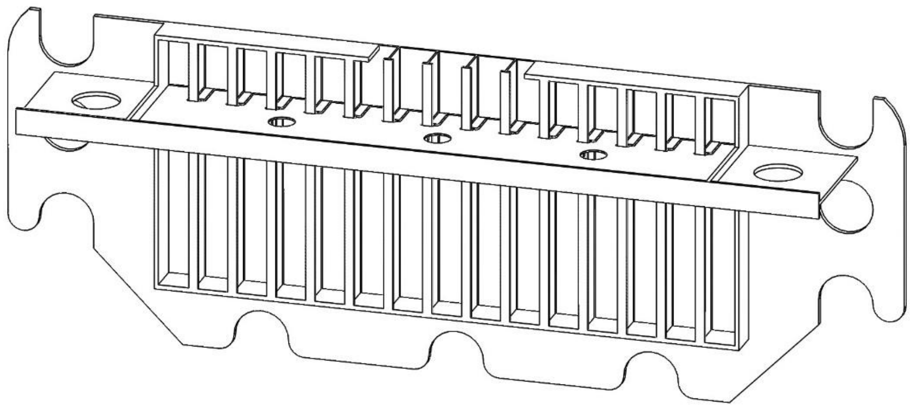

Fig. 4. Geometry of model structure.

4.2. Manufacture

The stainless steel 316L was used for the additively manufacturing of the miniature ship bottom structure. The structure was manufactured with a SLM 280 2.0 machine using a powder bed fusion process in which a laser beam generates the part by melting layers of metal powder, slice by slice, according to an input CAD geometry considering a layer thickness of 30 µm. The miniature structure was printed considering an upside down orientation, inclined 45 degrees, so aiming to minimize the amount of supporting structures in the more complex areas (between the stiffeners) as observed in Fig. 5 where the miniature structure is still attached to the printing platform.

After printing, the structure is subjected to a stress relief treatment (heating up to 600°C and cooled down slowly) and then detached from the base using a miter band saw, Fig. 5. Finally, the remaining supporting structures are manually removed and the structure is blast cleaned so gaining a sandblasted appearance, Fig. 6.

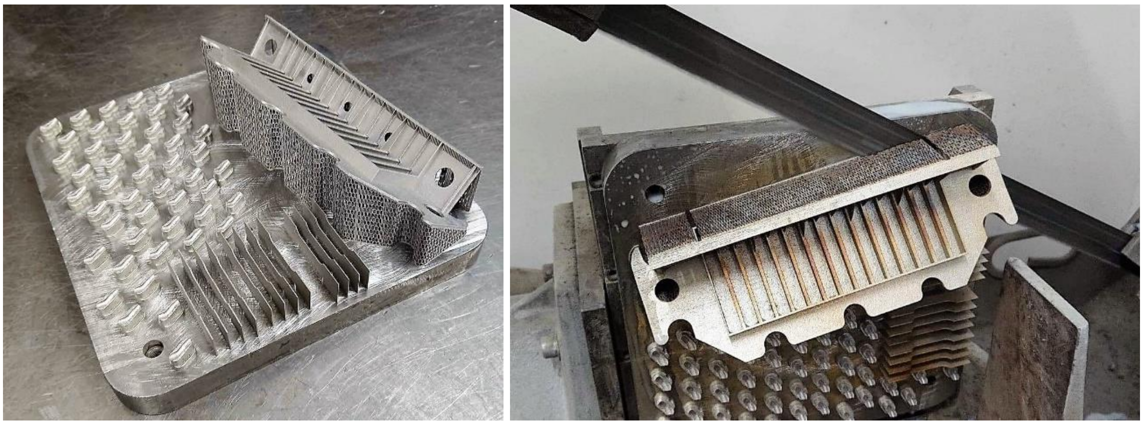

Fig. 5. Miniature structure attached to the base and during removal after stress relief treatment.

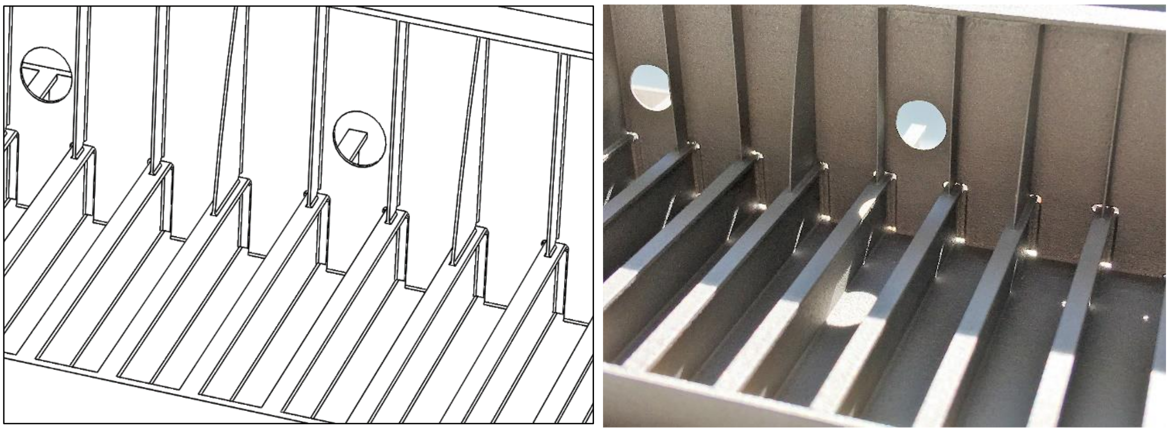

Fig. 6. Structural details in miniature structure: original design and manufactured structure.

4.3. Dimensional accuracy

The geometry of the printed structure was measured using an ATOS Core 3D (GOM mbH, Germany) and compared against the original designed CAD geometry in the GOM Inspect V7.5 SR2 (GOM mbH, Germany) software. In general, the dimensional accuracy of the printed structure resulted to be very precise with differences below 1.7%. However, the printed structure presented a slight overall bending, probably generated by the residual stresses induced during its manufacture. The higher rigidity of the central stiffened area reduced its local bending distortion (vertical distortion below 0.36 mm) while the non-stiffened edges presented a pronounced warping (maximum edge displacement of 1.2 mm). Since the edges have barely fastening function, their warping will not affect the structural response.

4.4. Mechanical characterization

In order to evaluate the strain hardening response of the printed 316L stainless steel material, and how the structure thickness influences it, uniaxial tensile tests were performed in samples with different thicknesses named as A, B and C (0.44, 0.57 and 0.72 mm respectively) and three samples per thickness (totaling nine samples). The samples are small flat dog-bone specimens with testing area of 25 mm length × 8 mm width. All samples were printed in horizontal orientation together with the miniature structure (Fig. 5a) considering the same printing parameters and post-processing sequence. Similarly to that made in previous works (Calle et al., 2019), the edges of the samples were smoothed using a small file and then by manual fine grinding with medium-to-fine sandpapers (from 80 to 120 grit sizes). All tensile tests were performed at a constant velocity of 0.02 mm/s (strain rates around 8.0×10^{-4} s^{-1}).

The true stress-strain curves were obtained using 2D Digital Image Correlation (DIC) technique. Digital photos were taken from the samples' surfaces, along the tests, at a constant rate of 1.0 frame/s. No surface preparation was necessary since the sample roughness resulted to be proper enough for the image post-processing. Since cracks initiate in different locals depending on the sample, stress-strain data were extracted in various sample's sections via the open-source software Ncorr v1.2 coupled with a Matlab routine. For every section, true stresses were computed as the total force divided by the actual section area, and, true strains, as the average of the logarithmic strains (ε_{yy}) in the same section.

Figure 7 presents the 2D strain fields of all samples just before failure occurrence and, besides, the resulting true stress-strain data for all samples at different sections. Earlier sample failures (A1 and B1) occurred due to the presence of preexistent imperfections in samples' edges as evidenced by their strain fields. Consequently, a strong dispersion in failure strains is obtained.

All samples presented common true stress-strain data up to their respective necking points. However, the stress levels resulted to be dependent on sample thickness being that thinner samples presented lower stress levels. The yield stresses and ultimate tensile strengths for all samples were estimated based on their engineering stress-strain curves (by $e = \exp[\varepsilon] - 1$ and $S = \sigma/[1 + e]$) and they are also presented in Fig. 7.

Previous works corroborated the low influence of the material's viscoplasticity on the mechanical response when modeling structural tests in quasi-static regime (Calle et al., 2019b). For this reason, no test for viscoplasticity analysis was included in the mechanical characterization.

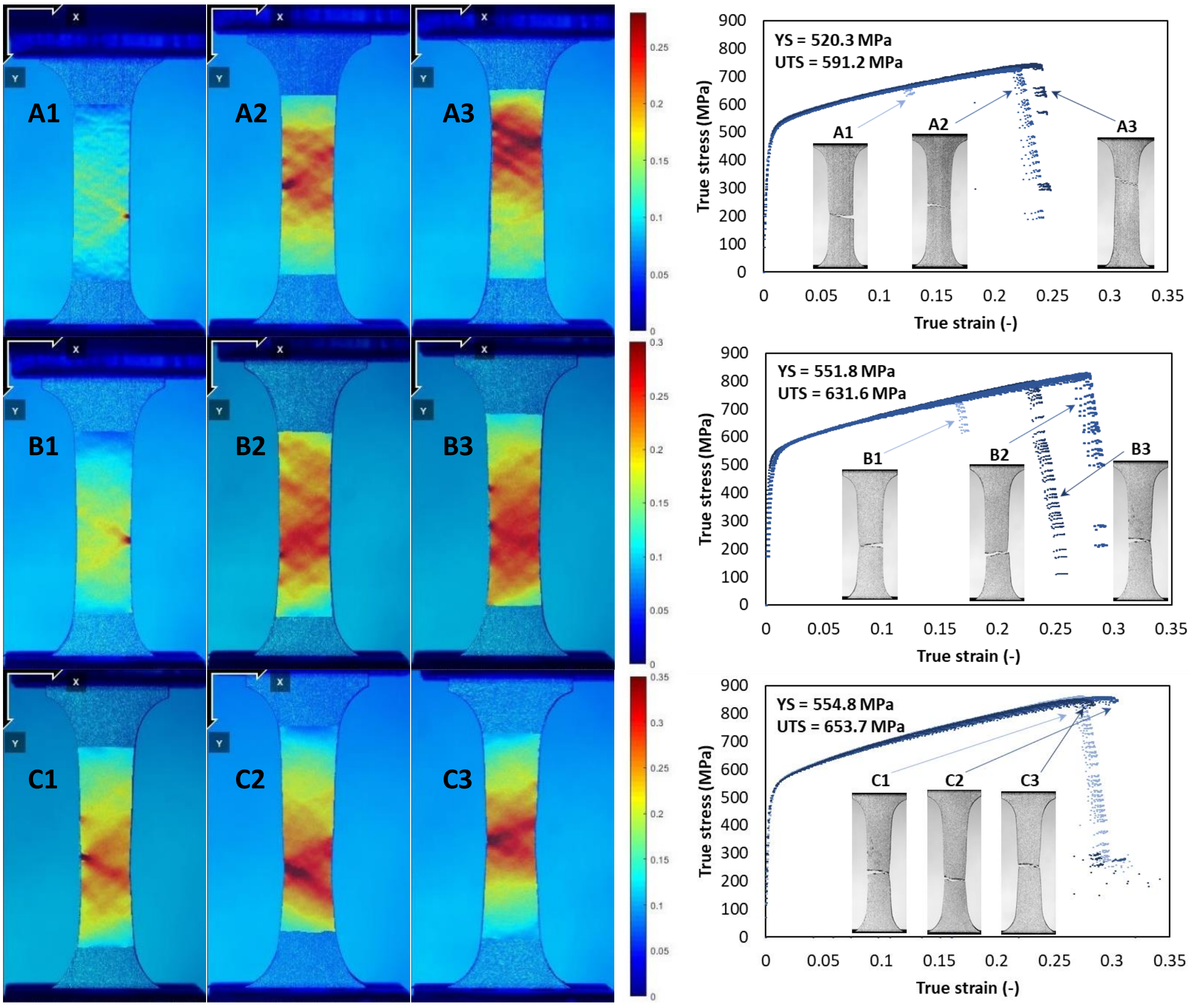

Fig. 7. Strain fields and stress-strain data of additively manufactured stainless steel 316L samples with different thicknesses: A (0.44 mm), B (0.57 mm) and C (0.72 mm).

Scanning Electron Microscopy (SEM) analyses were performed in the fractured sections of the tensile tests' samples to better evaluate the material rupture. A Zeiss Sigma VP microscope with a resolution of 1.3 nm at 20 kV was used for the analysis. The fractured sections of all samples presented a surface pattern of elongated dimples as seen in Fig. 8d typically found in ductile fracture. Traces of void formations are also clearly observed in all the fractured sections. Most of the larger voids initiated around non-sintered metal powder (pointed with white arrows in Figures 8a-c) as also observed in other works (Casati et al., 2016; Zhong et al., 2016; Hartunian and Eshraghi, 2018). Samples that presented early crack initiation before rupture (such as samples A1 and B1) also showed voids formation around non-sintered powder in the area of crack initiation (lateral edge of fractured section) as pointed in Fig. 8c.

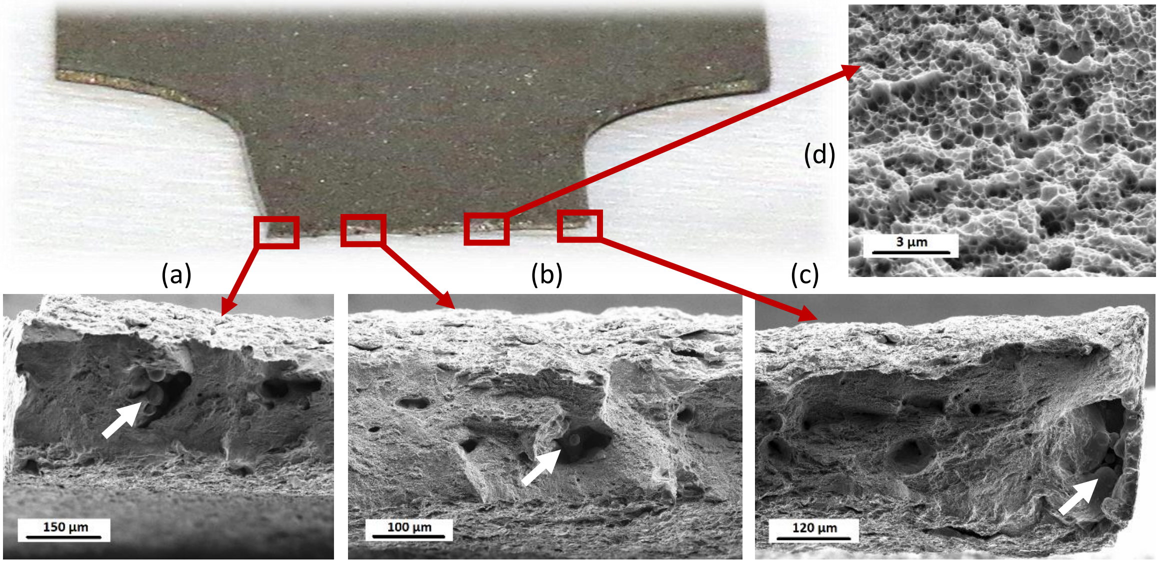

Fig. 8. SEM images extracted from fractured section of A1 tensile test sample.

5. Miniature raking test

5.1. Experiment

The tearing test of the miniature ship bottom structure was carried out in a universal testing machine Instron 3369 (50 kN capacity) at a test velocity of 0.1 mm/s. A sharp metallic solid indenter with 90° nose was used for the test accordingly to the reference large-scale test. A solid aluminum rig was built to fix the miniature structure during the test by clamping its lateral and bottom edges. The tearing process of the miniature structure was photo recorded during the test at a rate of 1.0 frame every 3 seconds using a D90 Nikon camera (12.3 megapixels) with Nikon lens model AF-S DX NIKKOR 18-105 mm f/3.5-5.6G.

The tearing process of both the bottom shell and the transversal ring face structures has the main role in the overall collapse mode. As longitudinal and transversal stiffeners underwent bending, but not up to rupture, they seemed to have a secondary role. Besides, a good correspondence in the progressive/overall tearing mechanism of the plate structure can be here corroborated when compared against its large-scale correspondent as observed in Fig. 9. Both prototype and model present side crushing of longitudinal stiffeners above transversal web, membrane tension rupture of transversal ring web and face, outward folding of longitudinal stiffeners below transversal web and the continuous tearing-opening process of the bottom shell by the sharp tip of the indenter.

However, when analyzing ruptured areas in the miniature model structure after the test via magnifier glass, a rupturing pattern different from that observed in wrought plates is found. Figure 10 shows two detailing views of material rupture in the bottom shell plate and the transversal ring face. Together with folding, these plates were torn and stretched up to rupture respectively. The folding process exposed a crackle pattern in the external surface of the plate while the internal surface wrinkled so indicating a plate core and surface layers with dissimilar mechanical responses.

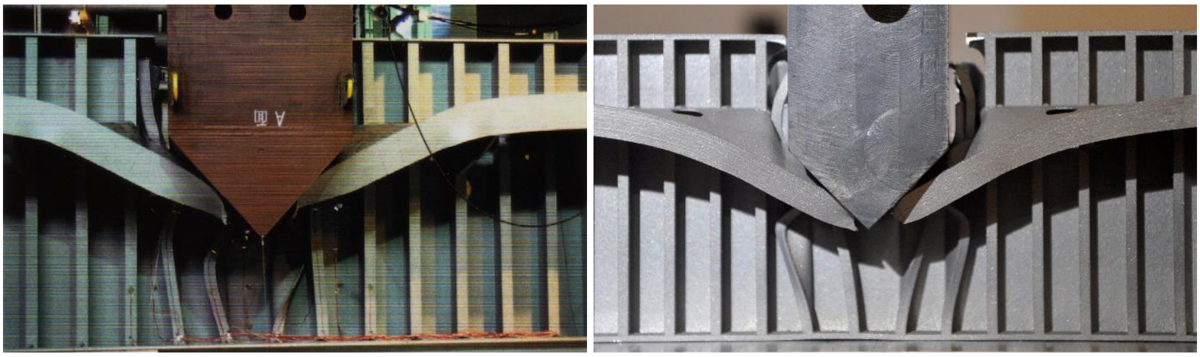

Fig. 9. Structural collapse of large-scale reference structure and 1:30 scaled model.

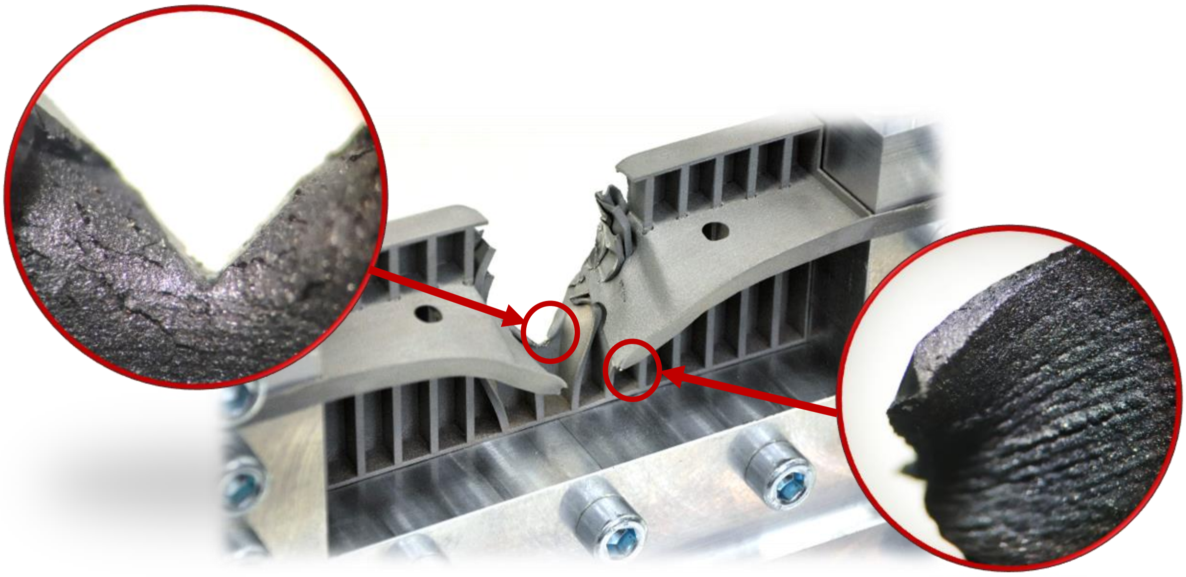

Fig. 10. Material rupture analysis in collapsed miniature model.

5.2. Structural response

To bring the mechanical response of the miniature model to its large-scale equivalent, the conversion factors for dimensional scaling and thickness distortion presented in Table 2 are employed. To evaluate them, β is defined as 1:30 (or β = 0.0333), η is 2.2 as previously assumed during structure design (thickness distortion), $\beta_{\sigma_{visco}}$ is assumed as 1.0 (quasi-static test) and β_{σ_0} is evaluated as a range (Eq. 1) from mechanical properties of prototype (σ_{y} = σ_0 = 315 MPa, σ_{UTS} = 408

MPa) and miniature model (0.57 mm thick sample: σ_{y} = 551.8 MPa, σ_{UTS} = 631.6 MPa) so resulting in β_{σ_0} = 1.685 ± 0.067. All resulting multiplying factors are summarized in Table 5.

Once brought to the same scale, the structural response of both miniature and large-scale structures are compared as presented in Fig. 11. As a whole, the force response of the miniature model presents an overall correspondence with that obtained from the large-scale reference, i.e., initial gradual increase of force reaction along indenter penetration before touching transversal ring and abrupt increase after touching it, stabilization of force level and oscillations during tearing of transversal ring and a slight decrease after that. However, the force response of the miniature model seems to be a little higher than that obtained from the large-scale test so generating a discrepancy in the total absorbed plastic energy of the miniature model and large-scale reference that achieves 7% at the maximum indenter penetration. This discrepancy could be enlarged by the multiple failures observed in the welded joints of the large-scale reference structure that reduced the overall structure strength as stated by Kuroiwa et al. (1992). The mechanical behavior of the fillet welding was not considered in the miniature modeling.

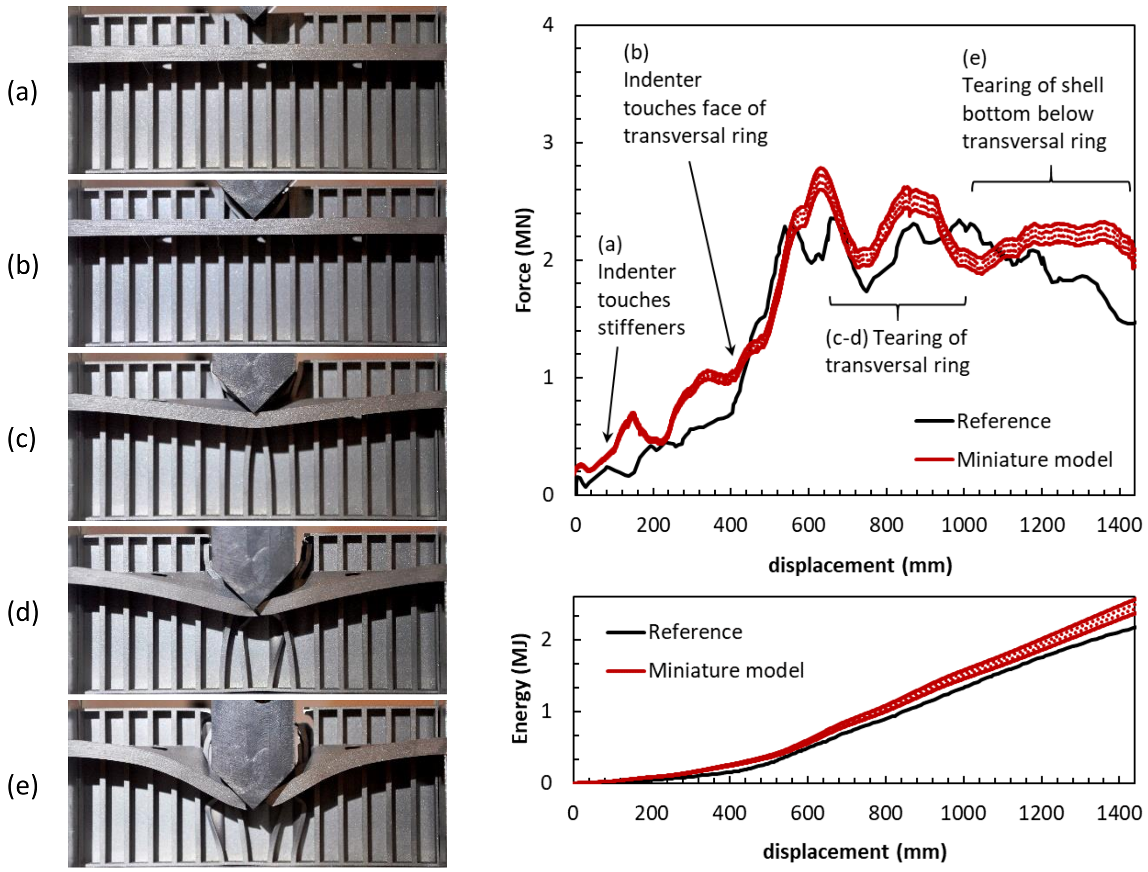

Fig. 11. Force and energy responses obtained from large-scale reference test and miniature model.

Table 5. Factors for dimensional scaling and thickness distortion.

Variable	Symbol	Factors
Length	β	0.0333
Thickness	η_t	See Table 4
displacement	β_δ	0.0333
Force	β_F	$[6.97 \pm 0.28]\times10^{-3}$
Energy	β_E	$[2.32 \pm 0.09]\times10^{-4}$

6. Conclusions

A technique to reproduce experimentally collision tests of large-scale marine structures via miniature models built by additive manufacturing is presented in this work. This technique relies on scaling laws and thickness distortion approaches. This experimental technique is validated by reproducing a large-scale raking test of a ship bottom structure as documented by Kuroiwa et al. (1992), but in a reduction scale of 1:30. The miniature thin-walled model structure was built by additive manufacturing in stainless steel 316L using powder bed fusion technique. Post-treatments of stress relief and blast cleaning were included.

The mechanical characterization of the material involved tensile tests in flat dog-bone samples with three different thicknesses together with microscopy analysis of the material fracture. These tests revealed a slight dependence of the stress-strain curves on the plate thickness and the early void formation during tensile stretching around non-sintered metallic powder. At the same time, the fracture area in the miniature structure presented crackle and wrinkled surface patterns in folded areas (external and internal surfaces of the fold respectively) so exposing a plate core and surface layer with different mechanical properties. It is still not clear in what degree this non-homogenous behavior influences the overall mechanical response of thin-walled structures.

In spite of that, a reasonable correspondence in the mechanical response of the large-scale test and the miniature model was achieved once brought to the same dimensional scale. Together with that, similar structural collapse aspects are clearly identifiable such as bottom shell tearing, lateral crushing of longitudinal stiffeners, overall bending and rupture of transversal ring among others. All of this confirms the validity of this technique when modeling raking tests.

Future works would need to focus on the improvement of the material quality of additively manufactured thin-walled metallic structures by considering different research fronts: modifying machine parameters to minimize non-sintered powder, improving surface quality and/or gaining a better understanding of the material failure so to be able to include new considerations in the similarity + geometry distortion technique.

7. Data availability

The STL geometry file of the miniature ship bottom structure and tensile test samples, the force displacement data from large-scale and miniature raking tests, SEM images, test setup images and miniature raking test video presented in this work are available to download from http://dx.doi.org/10.17632/cy994b3rvb.1.

8. Acknowledgment

The authors would like to thank the staff members of the GMSIE-EPUSP (Group of Solid Mechanics and Structural Impact of the Polytechnic School of the University of Sao Paulo) and of the Department of Mechanical Engineering of Aalto University for their valuable cooperation.

Appendix A

A.1 Membrane tension: Force induced by out-of-plane central force in plate and strip

$F(\delta) = 1.155 \frac{4n^2}{2n-1} \sigma_0 t \delta \left(\frac{b-b_0}{2a-2a_0} + \frac{a-a_0}{2b-2b_0} + \frac{b_0}{a-a_0} + \frac{a_0}{b-b_0} \right)$ (Zhang, 1999)

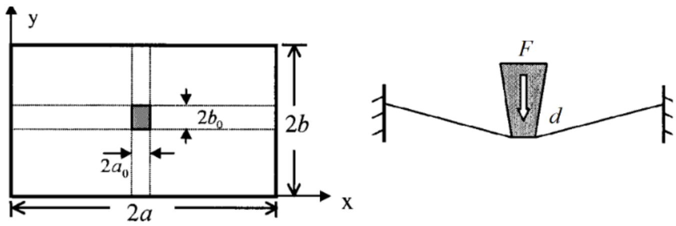

$F(\delta) = 1.15 \frac{n^2}{2n-1} \sigma_0 t \delta^2 \left(\frac{2b}{a_1} + \frac{2b}{a_2} \right)$ (Zhang, 1999)

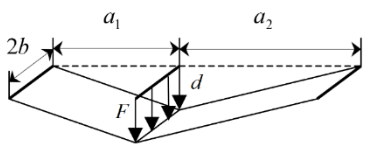

A.2 Folding: Average force induced by in-plane load in lateral of plate

$\bar{F} = 4.33\sigma_0 t^{5/3} b^{1/3}$ (Zhang, 1999)

$\bar{F} = 4.68\sigma_0 t^{5/3} b^{1/3}$ (Simonsen and Ocakli, 1999)

$\bar{F} = 4.25\sigma_0 t^{5/3} b^{1/3}$ (Hong and Amdahl, 2008)

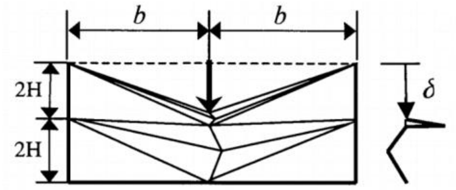

A.3 Tearing: Force induced by plate tearing cut by a wedge

$F(L) = 1.5 g_1(\theta)\sigma_0 t^{3/2} L^{1/2}$ (Paik, 1994)

$F(L) = 1.51 g_2(\theta)\sigma_0 t^{3/2} L^{1/2}$ (Ohtsubo and Wang, 1995)

$F(L) = 1.942 g_3(\theta)\sigma_0 t^{3/2} L^{1/2} \varepsilon_f^{1/4}$ (Zhang, 2002)

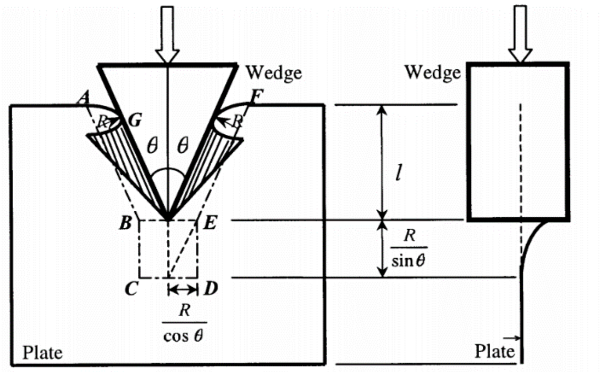

References

Calle, M.A.G., Oshiro, R.E., Alves, M., Ship collision and grounding: Scaled experiments and numerical analysis, International Journal of Impact Engineering, Vol. 103, pp. 195-210, 2017.

Calle, M. A. G., Salmi, M., Mazzariol, L. M., Alves, M., Kujala, P., Additive manufacturing of miniature marine structures for crashworthiness verification: Scaling technique and experimental tests, manuscript submitted for publication, 2019.

Casati, R., Lemke, J., Vedani, M., Microstructure and Fracture Behavior of 316L Austenitic Stainless Steel Produced by Selective Laser Melting, Journal of Materials Science & Technology, Vol. 32, n. 8, pp. 738-744, 2016.

Hartunian, P., Eshraghi, M., Effect of Build Orientation on the Microstructure and Mechanical Properties of Selective Laser Melted Ti-6Al-4V Alloy, Journal of Manufacturing and Materials Processing, 2, 69; 2018.

Hong, L., Amdahl, J., Crushing resistance of web girders in ship collision and grounding, Marine Structures, Vol. 21, pp. 374-401, 2008.

ISO/ASTM 52900:2015 (ASTM F2792), Additive manufacturing - General principles - Terminology, International Standard ISO/ASTM, first edition, December 2015.

Jordan, C.R., Krumpen, R.P. Jr., Design guide for ship structural details, SSC-331, Ship Structure Committee, Washington D.C., 132 p., 1985.

Kretzschmar, N., Chekurov, S., Salmi, M., & Tuomi, J., Evaluating the Readiness Level of Additively Manufactured Digital Spare Parts: An Industrial Perspective, Applied Sciences, Vol. 8, 1837, 2018.

Kuroiwa, T., Kawamoto, Y., Yuhara, T., Study on damage of ship bottom structure due to grounding, Proceedings of the First Joint Conference on Marine Safety and Environment Ship Production, Ship, Port and Offshore Technology, Delft University of Technology, 1992, Delft, The Netherlands.

Kuroiwa, T., Kusuba, S., Study on structural toughness against bottom raking due to grounding, Proceedings of the 16th International Conference on Offshore Mechanics and Artic Engineering (OMAE-1997), 1997, Yokohama, Japan.

Liu, B., Pedersen, P.T., Zhua, L., Zhang, S., Review of experiments and calculation procedures for ship collision and grounding damage, Marine Structures, Vol. 59, pp. 105–121, 2018.

Mazzariol, L.M., Oshiro, R.E., Alves, M., A method to represent impacted structures using scaled models made of different materials, International Journal of Impact Engineering, Vol. 90, pp. 81-94, 2016.

Ohtsubo, H., Kawamoto, Y., Kuroiwa, T., Experimental and numerical research on ship collision and grounding of oil tankers, Nuclear Engineering and Design, v. 150, n. 2–3, pp.385-396, 1994.

Ohtsubo H., Wang G., An upper-bound solution to the problem of plate tearing, Journal of Marine Science and Technology, Vol. 1, pp. 46–51, 1995.

Oshiro, R.E., Calle, M.A.G., Mazzariol, L.M., Alves, M., Experimental study of collision in scaled naval structures, International Journal of Impact Engineering, Vol. 110, pp. 149-161, 2017.

Paik J.K., Cutting of a longitudinally stiffened plate by a wedge, Journal of Ship Research, Vol. 38, n. 4, pp. 340–348, 1994.

Simonsen, B.C., Ocakli, H., Experiments and theory on deck and girder crushing, Thin-walled Structures, Vol. 34, pp. 195-216, 1999.

Tabri, K., Määttänen, J. and Ranta, J., ‘Model-scale experiments of symmetric ship collisions’, Journal of Marine Science and Technology, Vol. 13, pp. 71-84, 2008.

Tabri, K., Matusiak, J., Varsta, P., Sloshing interaction in ship collisions – An experimental and numerical study, Ocean Engineering, Vol. 36(17–18), pp. 1366-1376, 2009.

Törnqvist, R., 'Design of crashworthy ship structures', PhD Thesis, Technical University of Denmark, 2003.

Zhang, S., The mechanics of ship collisions, PhD Thesis, Department of Naval Architecture and Offshore Engineering, Technical University of Denmark, 1999.

Zhang, S., Plate tearing and bottom damage in ship grounding, Marine Structures, Vol. 15, pp. 101-117, 2002.

Zhong, Y., Liu, L., Wikman, S., Cui, D., Shen, Z., Intragranular cellular segregation network structure strengthening 316L stainless steel prepared by selective laser melting, Journal of Nuclear Materials, Vol. 470, pp. 170-178, 2016.

Zhu, L., Zhou, Q., Chen, M., Chen, X., ‘Grounding Experiments of a Ship Model in Water Tank’, Proceedings of the ASME 2018 (37th International Conference on Ocean, Offshore and Arctic Engineering), Vol. 11A: Honoring Symposium for Professor Carlos Guedes Soares on Marine Technology and Ocean Engineering, Madrid, 2018.